nature communications

Article

https://doi.org/10.1038/s41467-025-61775-1

Chemical circularization of in vitro transcribed RNA for exploring circular mRNA design

Received: 29 July 2024

Accepted: 27 June 2025

Published online: 12 July 2025

Check for updates

Malgorzata Wasinska-Kalwa[1,9], Adam Mamot[1,2,8,9], Karol Czubak[3], Katarzyna Frankowska[1], Adam Ado Rajkiewicz[1], Tomasz Spiewla[1,2], Marcin Warminski[2], Zofia Pilch[4], Marta Szulc-Gasiorowska[1], Kacper Siekan[5], Andrzej Dziembowski[6,7], Dominika Nowis[3], Jakub Golab[4], Joanna Kowalska[2] ✉ & Jacek Jemielity[1] ✉

Circularization is an important step for therapeutic messenger RNA (mRNA) enhancements. Current enzymatic and ribozymatic-based circularization methods face limitations including sequence constraints, purification challenges, and sub-optimal biological activity. Chemical strategies, while promising, have been restricted to short RNA sequences. Here, we report a method for chemically circularized in vitro transcribed RNAs of various lengths (chem-circRNAs; 35–4000 nt) with circularization efficiencies reaching up to 60%. This approach leverages a 5′ ethylenediamine modification and a periodate-oxidized 3′ end to drive intramolecular reductive amination. We demonstrate that this method is applicable to various sequences and modification compatible. We report the effective separation methods of chem-circRNAs from their linear precursors. We show that protein-coding chem-circRNAs are translationally active in cells and exhibit increased durability, like enzymatically circularized mRNAs. Furthermore, our method allows incorporation of functional modifications, including endocyclic N7-methylguanosine cap and N1-methylpseudouridine, enabling access to chemically defined translationally active circRNAs for therapeutic applications.

Despite its inherent fragility, mRNA is one of the most prolific substances in the context of therapeutic gene delivery[1]. To ensure sufficient biological activity of therapeutic mRNA, it is necessary to protect it from premature cleavage by numerous RNA-targeting enzymes, particularly exonucleases[2]. Circularization is one of the most promising modifications of mRNA in this context, as it prevents exonucleolytic digestion[3,4]. Consequently, circRNAs have shown higher stability than corresponding linear RNAs and exhibited significantly longer protein expression profiles[5–7]. Unfortunately, the circularization of macromolecular RNA still poses a significant challenge.

Currently established methods of RNA circularization are based on chemical reactions, enzymatic reactions, or the activity of

[1]Centre of New Technologies, University of Warsaw, Banacha 2c Street, 02-097 Warsaw, Poland. [2]Division of Biophysics, Institute of Experimental Physics, Faculty of Physics, University of Warsaw, Pasteura 5 Street, 02-093 Warsaw, Poland. [3]Laboratory of Experimental Medicine, Medical University of Warsaw, Nielubowicza 5 Street, 02-097 Warsaw, Poland. [4]Department of Immunology, Medical University of Warsaw, Nielubowicza 5 Street, 02-097 Warsaw, Poland. [5]Genome Engineering Facility, International Institute of Molecular and Cell Biology, 4 Ks. Trojdena, 02-106 Warsaw, Poland. [6]Laboratory of RNA Biology, International Institute of Molecular and Cell Biology, 4 Ks. Trojdena, 02-106 Warsaw, Poland. [7]Department of Embryology, Faculty of Biology, University of Warsaw, 1 Miecznikowa, 02-096 Warsaw, Poland. [8]Present address: Max Planck Institute of Biochemistry, Am Klopferspitz 18, 82152 Martinsried, Germany. [9]These authors contributed equally: Malgorzata Wasinska-Kalwa, Adam Mamot. ✉e-mail: jkowalska@fuw.edu.pl; j.jemielity@cent.uw.edu.pl

https://doi.org/10.1038/s41467-025-61775-1

autocatalytic RNA sequences[8]. The chemical circularization methods rely on short precursor RNA sequences, synthesized via phosphoramidite chemistry[9–11]. In consequence, the so-far chemically synthesized circRNAs encoded relatively short sequences and have limited use in the context of therapeutic gene delivery. Alternatively, RNA circularization can be carried out with ligases, such as T4 RNA ligase I and T4 RNA ligase II (Fig. 1A)[12–14]. Both enzymes require 5′ monophosphorylated precursors that are first adenylated and subsequently ligated with the 3′ OH of the ribose at the 3′ end RNA. The ligases are strongly dependent on the target RNA length and sequence[5,6,14,15]. As a result, it is difficult to predict or improve the performance of such enzymes. Other methods of RNA circularization involve catalytic nucleic acids (Fig. 1A)[5,6,16–19]. Wesselhoeft et al. have circularized RNA in vitro by using the permuted intron-exon (PIE)

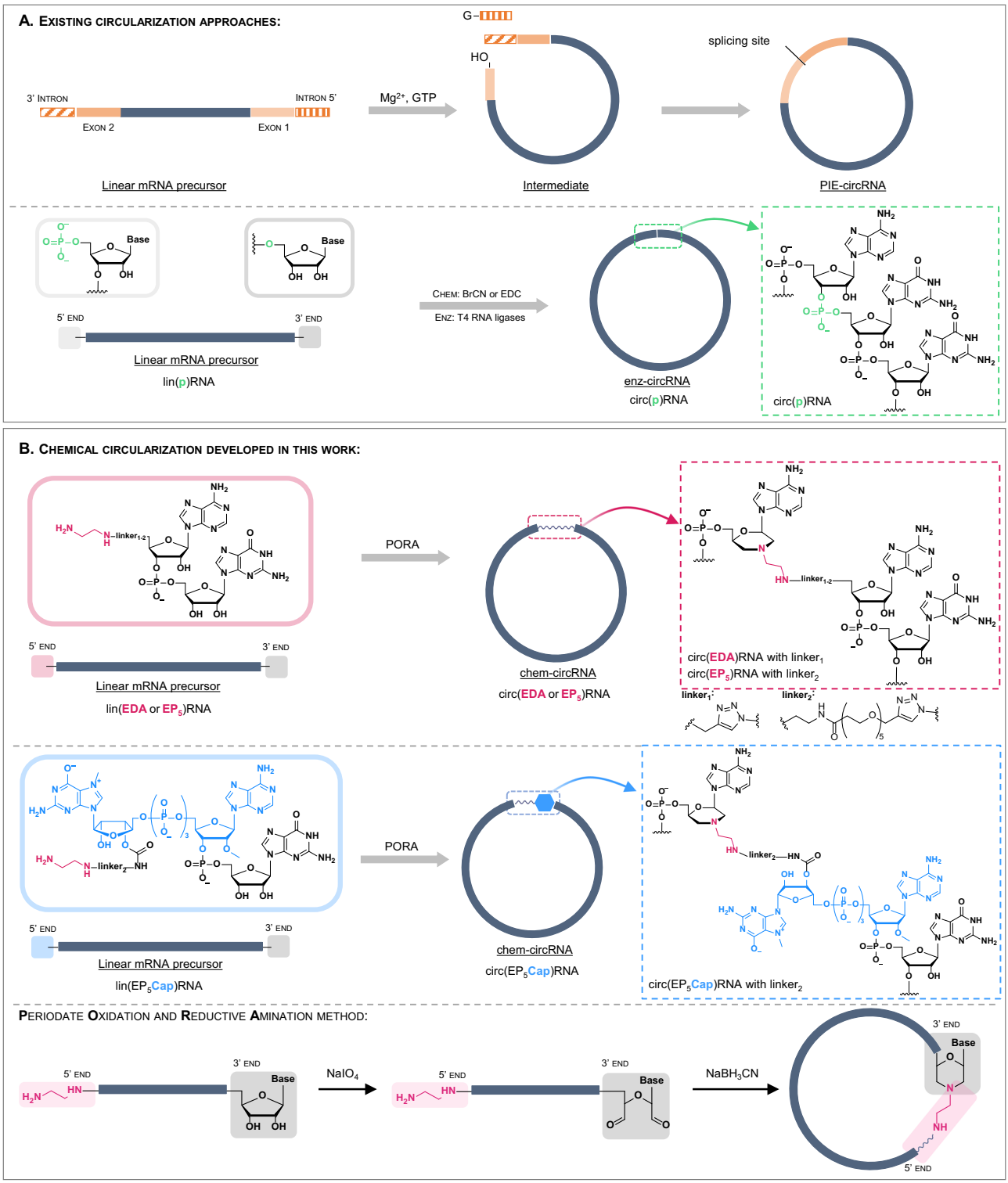

Fig. 1 | Strategies for RNA circularization. A Overview of existing circularization approaches. **B** Chemical circularization developed in this work. The 5′ modified linear RNA precursor is obtained from a 5′ initiator (EDA-AG, EP_5AG or EP_5Cap) during an in vitro transcription (IVT) reaction and is subsequently circularized by PORA reaction. The produced circRNA contains a single chemically modified linkage.

system and optimized self-splicing intronic sequences[5,6]. Litke et al. have shown the Twister-optimized RNA durable overexpression (Tornado) system for RNA circularization in cells[16]. These methods are based on sequence-dependent activity and can be hindered by methylated nucleobases [e.g. N1-methylpseudouridine ($m^1\Psi$) or N6-methyladenosine] and other chemical modifications[6]. Moreover, the translation of currently known circRNAs relies on internal ribosome entry site (IRES) sequences[20,21]. It is well-established that, for linear mRNAs, translation driven by an IRES sequence is less efficient than the main pathways of eukaryotic translation involving cap-and-poly(A)-dependent initiation[22–25]. Hence, robust and scalable methods of RNA circularization that are compatible with mRNA body modifications or cap-dependent translation mechanisms are strongly desired.

In this work, we develop a chemical circularization method that expands circ-mRNA design strategies beyond IRES-dependent translation. Taking advantage of the unique reactivity of the ethylenediamine moiety towards oxidized RNA 3′ ends, we establish a post-transcriptional circularization protocol relying on a one-pot, two-step chemical reaction (Fig. 1B)[26–29]. The protocol is based on affordable, readily available, non-invasive reagents and can be applied to RNA of virtually any size and sequence (Fig. 1B). This approach, combined with improved purification and isolation techniques, provides access to chem-circRNAs of up to 4000 nt. mRNAs generated using our approach are evaluated in living cells to determine their relative stability and translational activity. We show that our circularization method is compatible with incorporating chemical modifications such as N7-methylguanosine cap and $m^1\Psi$. Our findings offer an alternative to chemoenzymatic methods of RNA circularization and promote circ-mRNA optimization.

Results

Development of the chemical circularization method

Our approach towards circRNAs was designed to minimize the number of steps necessary to functionalize and circularize the target RNA, maintaining the process as close as possible to the existing mRNA production pipelines. In the first step, we generate an in vitro transcribed (IVT) pre-circRNA that is 5′ functionalized with ethylenediamine by incorporating a properly designed transcription initiator (primer; Fig. 1B). Such pre-circRNA is then post-transcriptionally circularized by one-pot periodate oxidation and reductive amination (PORA) reaction, resulting in the formation of a morpholine-derived inter-nucleotide linkage (Fig. 1B). As transcription initiators, we designed two types of AG dinucleotides equipped with ethylenediamine linkers (EDA-linkers) of different lengths– EDA-AG (EDA) and EDA-PEG_5-AG (EP_5) (Fig. 1B). We also designed an EDA-functionalized cap 1 analog – EDA-PEG_5-m^7GpppA_mG (EP_5Cap)—to provide unprecedented access to circular mRNAs containing an endocyclic 5′ cap structure (Fig. 1B). The presence of circular RNAs was verified by polyacrylamide gel electrophoresis (PAGE) and compared to analogous circRNA obtained by enzymatic ligation (Supplementary Fig. 1).

The synthesis of the primers was performed in a single synthetic step using click chemistry (NHS-based amidation and CuAAC) from an azido-modified dinucleotide synthesized on solid-support (N_3-AG, Supplementary Fig. 2).

We began our attempts at chemical RNA circularization using two RNA oligonucleotide models: (EDA)RNA_{01} and (EDA)RNA_{02}, (35 nucleotide-long sequences, Table 1, Fig. 2), transcribed in the presence of EDA-AG initiator (Fig. 1B, Supplementary Fig. 2). The transcription products were obtained in reasonable yields and quality, suggesting successful generation of RNA with functionalized 5′ end (the heterogeneity observed as multiple bands on the PAGE gel is typical for in vitro transcription, which generates mRNA products of various sizes, primarily due to non-templated nucleotide additions at the 3′ and 5′ ends)[30].

The subsequent step of chemical circularization was based on our previous findings that oxidized RNA 3′ ends show particularly high reactivity in PORA reactions toward compounds containing ethylenediamine[26]. To execute the PORA reaction, (EDA)RNA_{01} and (EDA)RNA_{02} were incubated in a sodium periodate ($NaIO_4$) solution, leading to the formation of an acyclic 2′,3′-dialdehyde at the 3′ terminal nucleotide. This derivative spontaneously reacted with the ethylenediamine motif to form a cyclic intermediate. The subsequent addition of sodium cyanoborohydride ($NaBH_3CN$) led to the reduction of the cyclic intermediate, ensuring the irreversibility of the reaction. As a result, a morpholine linkage was formed between the former 3′ terminal nucleotide and the 5′ terminus of the transcription initiator (Fig. 2).

To test the scope and limitations of this reaction, we first investigated the basic factors affecting chemical circularization. To that end, we tested the influence of pH, temperature, and RNA concentration on the circularization yield.

The circularization efficiencies were estimated by PAGE combined with densitometric analyses (Fig. 2 and Supplementary Fig. 3). To minimize bias arising from the arbitrary selection of main band(s) (for product or substrate) and to reduce errors from incorrect intensity calculations (caused by overlapping peaks or challenges in baseline assignment), the entire regions corresponding to the substrates and products of circularization (sum of the six main peaks) were used in our calculations. We observed that the conversion of linear precursor (~50%) was not significantly affected by pH (5.6–8.0) (Supplementary Fig. 3), time, temperature (2 h at 20 °C or 16 h at 4 °C), or the concentration of the precursor (0.3–12 μM) (Fig. 2A). However, both RNA sequence and concentration were crucial for circularization selectivity. The circularization of (EDA)RNA_{01} was, on average, more selective (50–70%) than that of (EDA)RNA_{02} (30–55%), which also produced linear and circular dimers. Notably, the circularization of (EDA)RNA_{01} did not lead to any linear and circular polymeric by-products (dimers and concatemers), especially at lower concentrations of RNA (Fig. 2A).

To gain insight into the sequence-dependence of RNAs circularization, secondary and tertiary structural models of the RNA_{01} and RNA_{02} sequences were generated using automated structure predictors (Fig. 2B–D)[31–33]. Computational predictions suggested that both RNA_{01} and RNA_{02} can form distinct secondary and tertiary structures. The structure of RNA_{01} features a stable hairpin (free energy of the thermodynamic ensemble −8.2 kcal/mol) with an open loop motif within which the 3′ and 5′ ends spatially converge. The predicted average distance between the 5′ and 3′ ends in the RNA_{01} model is shorter (2.3 nm), making the molecule prone to circularization (Fig. 2B). In contrast, the secondary structure of RNA_{02} formed a low stability hairpin (−5.1 kcal/mol). The 3′ and 5′ ends reside within a bigger open loop, with an increased end-to-end distance (4.9 nm). Moreover, the tertiary structure model of RNA_{02} suggested that the 3′ and 5′ ends could point in opposite directions (Fig. 2C). The spatial arrangement of these termini probably enhances the likelihood of intermolecular interactions rather than intramolecular ones, ultimately leading to the preferential formation of stable RNA dimers (−18.3 kcal/mol), especially at higher concentrations (Fig. 2A, D). Overall, the chemical circularization method worked well on the oligonucleotide models, and its selectivity and efficiency could be rationalized with the help of computational methods. Considering that the majority of long RNA sequences adopt tertiary structures with termini separated by no more than 10 nm, these results encouraged us to test circularization on longer RNAs[34].

To that end, we performed chemical circularization of macromolecular RNAs (RNA_{03}–RNA_{08}, 276–760 nt), which included various protein-coding RNAs or their 5′ terminal fragments (Table 1). Here, we took advantage of a dinucleotide initiator with a longer linker (EP_5AG; Supplementary Fig 2). The chemical circularization process proceeded quite efficiently for most of the studied sequences, independent of their length, yielding circularization efficiencies ranging from 47% to 60% (Table 1). The chemical circularization yield was generally lower for RNAs longer than 900 nt compared to shorter RNAs (Table 1; compare RNA_{04} versus RNA_{09}). Furthermore, the introduction of a poly(A) sequence (A_{30}) at the 3′ end of the precursor resulted in a

https://doi.org/10.1038/s41467-025-61775-1

Table 1 | Summary of precursor RNA sequences (abbreviation, sequence elements, length, and circularization method) and circularization yields according to circularization reaction (chemical PORA, enzymatic with, T4 RNA ligase II or autocatalytic PIE) with or without (w/o) splint DNA oligonucleotides

RNA sequence	RNA sequence elements[a]				RNA length	Circularizationmethod	IVT initiator	oligoDNA	Circ. yield[c] [%]
	5′ UTR	CDS	3′ UTR	3′ tail					
RNA_{01}	AGGGAAGCGGGCAUGCGGCCAGCCAUAGCCGAUCA				35	PORA	EDA-AG	w/o	50–70
RNA_{02}	AGGUCAGAACGAGCGAGCGGCCAUAUGAGCAUGCA				35	PORA	EDA-AG	w/o	30–55
RNA_{03}	MCS	RLuc [b]	–	–	276	PORA	EP_5AG	w/o	60
RNA_{04}	Kozak	eGFP	–	–	760	PORA	EP_5AG	w/o	47
								ON0	49
RNA_{05}	Kozak	GLuc	–	–	578	PORA	EP_5AG	w/o	60
							EP_5Cap		53
RNA_{06}	RSV	GLuc	–	–	598	PORA	EP_5AG	w/o	52
RNA_{07}	OligoIRES	GLuc	–	–	711	PORA	EP_5AG	w/o	53
RNA_{08}	HBB	GLuc	–	–	626	PORA	EP_5Cap	w/o	46
RNA_{09}	Kozak	GLuc	HBB x2	A_{30}	908	T4 Lig. II	GMP	ON5	43
						PORA	EP_5Cap	w/o	2
								ON5	57
RNA_{10}	HBB	GLuc	HBB x2	–	918	T4 Lig. II	GMP	ON6	45
						PORA	EP_5Cap	w/o	33
							EP_5AG	ON6	63
							EP_5Cap		53
RNA_{11}	HBB	GLuc	HBB x2	A_{30}	952	T4 Lig. II	GMP	ON2	61
						PORA	EP_5Cap	w/o	2
							EP_5Cap	ON2	57
RNA_{12}	EMCV	GLuc	–	–	1154	T4 Lig. II	GMP	ON7	46
						PORA	EP_5Cap	w/o	41
							EP_5AG	ON7	46
							EP_5Cap		52
RNA_{13}	EMCV	GLuc	–	A_{30}	1207	T4 Lig. II	GMP	ON8	40
						PORA	EP_5Cap	w/o	0
							EP_5AG	ON8	53
							EP_5Cap		57
RNA_{14}	EMCV	GLuc	HBB x2	–	1446	T4 Lig. II	GMP	ON9	52
						PORA	EP_5Cap	w/o	4
							EP_5AG	ON9	45
							EP_5Cap		35
RNA_{15}	EMCV	GLuc	HBB x2	A_{30}	1481	T4 Lig. II	GMP	ON8	56
						PORA	EP_5Cap	w/o	1
							EP_5AG	ON8	35
							EP_5Cap		55
RNA_{16}-PIE[c]	EMCV	GLuc	spacers		1612	PIE	–	–	54
RNA_{17}	from BNT162b	Spike	–	–	3893	T4 Lig. II	GMP	ON10	25
						PORA	EP_5AG	w/o	0
								ON10	35
RNA_{18}	HBB	hEPO	30 nt (HBB)	–	688	PORA	EP_5Cap	w/o	56
								ON11	50
RNA_{19}	EMCV	hEPO	30 nt (HBB)	–	1221	PORA	EP_5Cap	w/o	21
								ON12	55

[a]MCS—a multiple cloning site (84 nt); Kozak—a sequence promoting translation (8–12 nt); HBB (human beta-globin)—a sequence derived from the human beta-globin gene (50 nt); RSV—a sequence promoting m^6A-mediated translation (MIRES) from respiratory syncytial virus (27 nt)[27]; EMCV—an IRES from encephalomyocarditis virus (583 nt)[5]; OligoIRES—an artificial IRES sequence (200 nt)[28].
[b]RLuc—sequence of the first 62 amino acids of *Renilla* luciferase (186 nt); eGFP—sequence encoding enhanced green fluorescence protein (720 nt); GLuc—sequence coding for *Gaussia-Dura* luciferase (558 nt); HBBx2—doubled sequence derived from human beta-globin gene (270 nt); A_{30}—polyadenine tail (30 nt); Spike form SARS-Cov-2 CDS sequence identical to BNT162b—(3893 nt)[29]; hEPO—sequence coding for human Erythropoietin (585 nt); 30 nt (HBB)—first 30 nt from HBB sequence.
[c]RNA sequence designed based on Wesselhoeft et al.[5,6] (linear mRNA precursor 1612 nt—for full PIE construct scheme see Supplementary Fig. 5). Content of mRNA species was quantified densitometrically using CLIQS (Core Laboratory Image Quantification Software).

https://doi.org/10.1038/s41467-025-61775-1

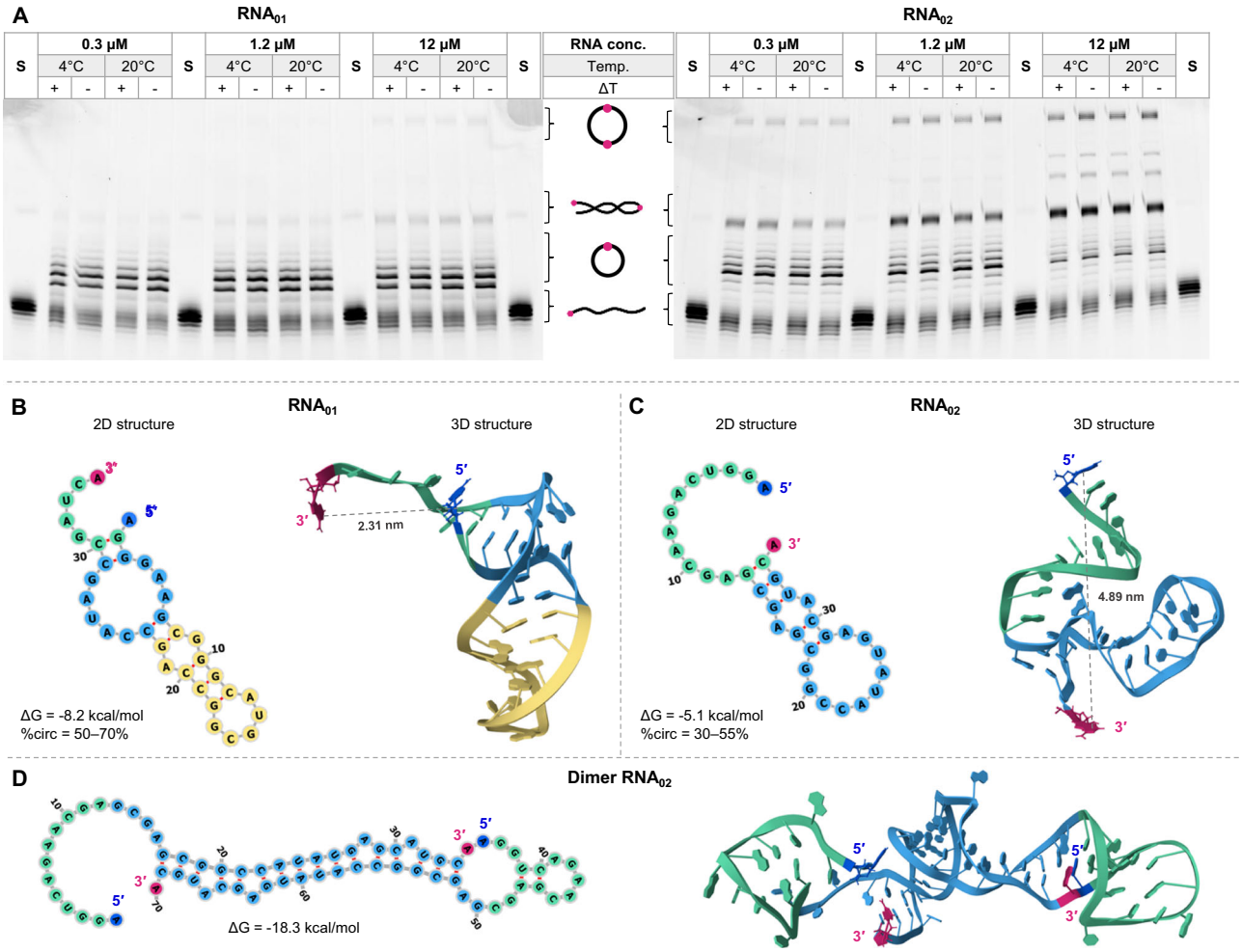

Fig. 2 | Optimization of chemical circularization of two RNA oligonucleotides (35 nt). A PAGE analysis of the circularization reaction of (EDA)RNA_{01} and (EDA) RNA_{02}. RNAs were circularized at concentrations of 0.3, 1.2, or 12 µM, at 4 or 20 °C, with (+ΔT) or without (−ΔT) thermal refolding (rapid heating and subsequent slow cooling) prior to circularization. S refers to an untreated RNA substrate. Data presented is representative of one independent experiment. **B**–**D** Minimum-free-energy (MFE) secondary structure (2D) models (predicted with RNAfold web server) and tertiary structure (3D) of predicted models (RNA Composer web server) for RNA_{01} (**B**), RNA_{02} (**C**), and RNA_{02} dimer (**D**). Content of mRNA species was quantified using CLIQS (Core Laboratory Image Quantification Software).

dramatic reduction in circularization yield (<5%). For instance, the circularization efficiency of RNA_{10}, which lacks the poly(A) (A_{30}), was 33%, whereas for the same sequence with the poly(A) (RNA_{11}), it was only 2%. A similar result was obtained for another sequence containing an A_{30} tract (RNA_{09}) (Table 1, Supplementary Fig. 4). The low efficiency of circularization for these sequences is likely due to the unstructured nature of the poly(A) region, which increases the 5′–3′ end-to-end distance in the precursor[34]. Since our overall goal was to develop a circularization method applicable to all RNA sequences and lengths, we attempted to overcome this issue by applying a splint-mediated approach. To decrease the distances between the 5′- and 3′-terminal moieties in longer and unstructured RNAs, we annealed the linear precursors with oligonucleotide DNA splints (short DNA sequences that are complementary to the 5′ and 3′ flanking regions of the precursor RNA; Fig. 3, Supplementary Table 2). To that end, we applied computational modeling (RNAfold web server) to RNA_{11} (952 nt) containing human beta globin (HBB) 5′ and 3′ UTRs, *Gaussia* luciferase (GLuc) ORF, and A_{30} tract, to design four DNA sequences differing in length and targeting specific structural features of the precursor RNAs (ON1-ON4; 10–67 nt; Fig. 3A, Supplementary Table 2). Next, we synthesized a molecular probe consisting of RNA_{11} labeled with a fluorescent FRET pair, Cy5 and Cy3, at the 5′ and 3′ ends, respectively (Fig. 3B)[26]. Measuring and analyzing the fluorescence spectra recorded at different temperatures, before and after splint annealing with the probe, led to the selection of an optimal splint sequence (ON2, 28 nt; Fig. 3). For RNA_{11}, the circularization efficiency in the presence of the optimal DNA splint (ON2, 28 nt, 50%) was over twenty-fold higher than that in the absence of DNA (2%) or in the presence of sub-optimal splints (2–40%, Fig. 3B, C). The use of longer DNA splints, ON3 (48 nt) and ON4 (67 nt), resulted in reduced circularization selectivity and increased linear RNA polymers formation (Fig. 3C), whereas the shorter splint (ON1, 10 nt) did not improve circularization efficiency at all. The experiment revealed that the optimal splint has to form a sufficiently stable RNA-DNA duplex (melting temperature ~50 °C) to unwind the less stable RNA-RNA secondary structure (melting temperature ~20–30 °C), but should not be too long as it shifts the equilibrium toward dimer formation (Fig. 3A). The addition of the splint improved circularization of RNAs longer than 900 nt but had no effect for shorter (760 nt) sequences (Table 1; see data for RNA_{04} or RNA_{18}).

To verify the universality of this splint-based approach for longer RNAs, we applied it to RNA sequences: RNA_{09}, RNA_{10} RNA_{12}-RNA_{19}. Our observations indicated that the efficiency of chemical circularization, particularly for sequences possessing a poly(A) tract, increased significantly in the presence of a suitably designed splint (Table 1). The longest RNA we attempted to circularize was 3893 nt long mRNA (RNA_{17}) encoding the BNT162b anti-COVID vaccine[29], achieving

https://doi.org/10.1038/s41467-025-61775-1

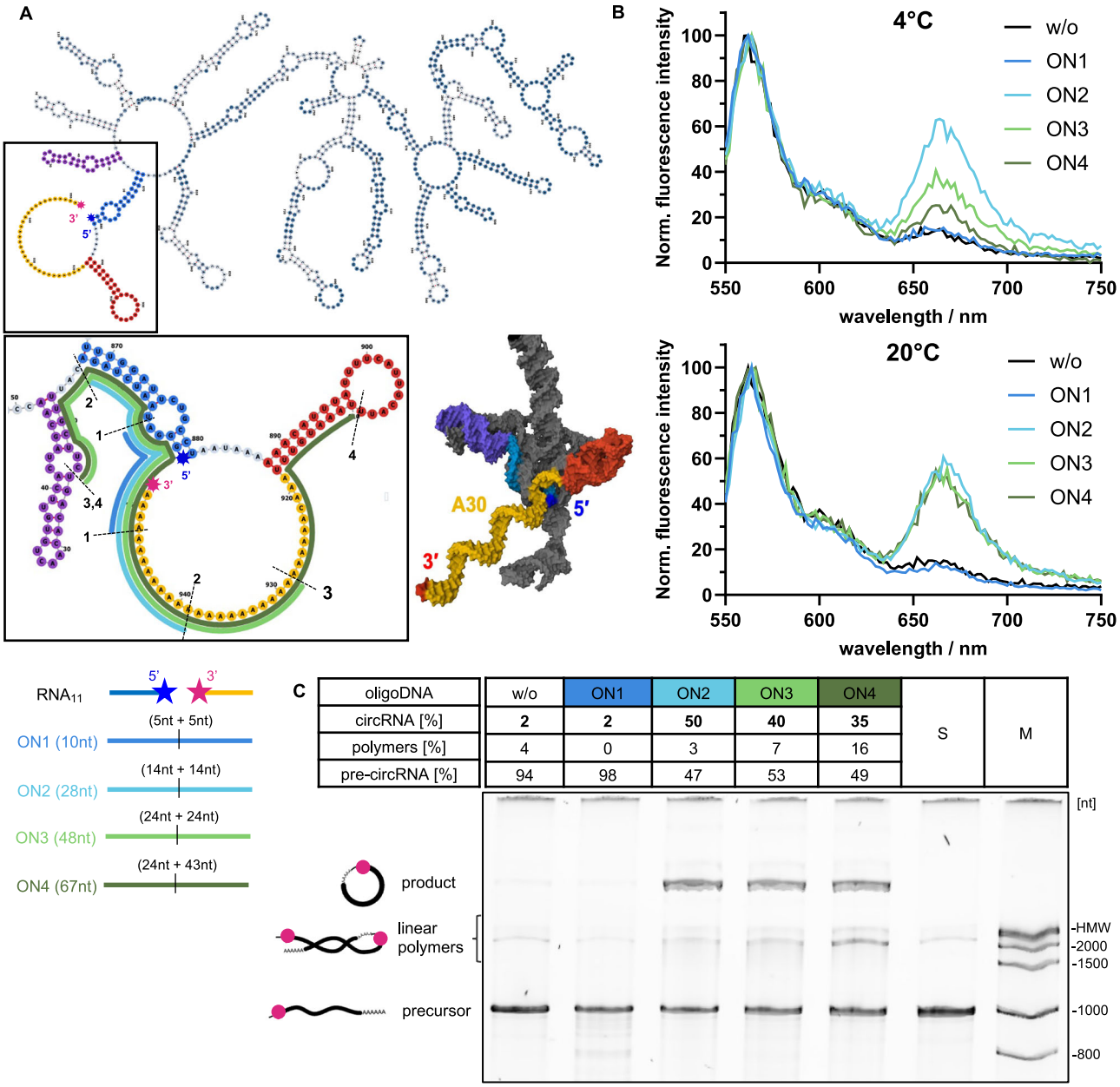

oligoDNA	w/o	ON1	ON2	ON3	ON4	S	M
circRNA [%]	**2**	**2**	**50**	**40**	**35**		
polymers [%]	4	0	3	7	16		
pre-circRNA [%]	94	98	47	53	49		

Fig. 3 | Circularization efficiency for challenging RNA sequences can be augmented using DNA splints and optimized by applying FRET probes and molecular modeling. A The predicted MFE secondary structure of RNA_{11} aligned with the tested DNA splints (ON1–4) and tertiary structure model of a selected fragment (predicted with RNAfold web server). Numbers 1–4 mark the regions of hypothetical interactions between RNA and the splints (Supplementary Table 2). **B** Fluorescence emission spectra (ex. 500 nm) of a FRET probe (Cy5-RNA_{11}-Cy3) after hybridization with oligonucleotide splints (ON1–4, Supplementary Table 2) or without splint (w/o), recorded at 4 °C or 20 °C. **C** PAGE analysis of the chemical products of RNA_{11} circularization, preformed after annealing the precursor with (ON1–4, Supplementary Table 2) or without (w/o) an oligonucleotide splint. S refers to the untreated precursor. Content of mRNA species was quantified densitometrically using CLIQS (Core Laboratory Image Quantification Software). Data presented is representative of one independent experiment.

successful chemical circularization also in this case, albeit with lower yield compared to shorter RNAs (35%).

Furthermore, during the circularization reaction, we observed little to no formation of polymeric side-products or nicking of the desired product. Overall, we found that splint-aided chemical circularization is equally efficient (44–63%) as the PIE methodology (54%, Supplementary Fig 5). Ligation of the respective mRNAs with T4 RNA ligase II yielded circularization efficiencies from 40 to 60% and were comparable to chemical circularization (Table 1). However, we noted that enzymatic ligation was significantly more sequence-dependent than chemical circularization. Since the circularization efficiency may be limited by the efficiency of co-transcriptional incorporation of the modified initiators, EP_5AG or EP_5Cap, we evaluated the incorporation (capping) efficiencies for one of the model RNAs. To that end, we performed ribozyme-mediated cleavage of $(EP_5)RNA_{11}$ and $(EP_5Cap)RNA_{11}$, and compared the results to uncapped (triphosphorylated) RNA_{11} [$(p_3)RNA_{11}$)]. The incorporation efficiency of the initiators was 94% and 87% for EP_5AG and EP_5Cap (Supplementary Fig 6), respectively, which may suggest that the circularization yield can be slightly improved by decreasing the content of uncapped RNA.

Analytical methods for identifying and isolating chem-circRNA

The purity and homogeneity of circular RNA are crucial for mitigating an innate immune response and ensuring sustained protein

https://doi.org/10.1038/s41467-025-61775-1

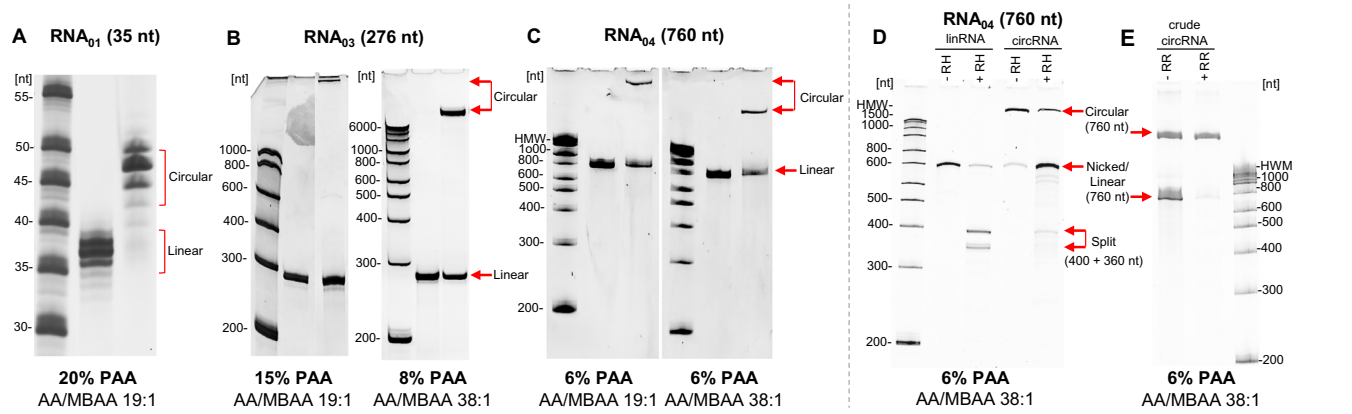

Fig. 4 | Electrophoretic and enzymatic methods for the analysis of chem-circRNA. A–C Resolution of circular RNAs and their linear precursors based on molecular size (**A** RNA_{01} 35 nt, **B** RNA_{03} 276 nt, **C** RNA_{04} 760 nt), gel density, and cross-linking degree of denaturing polyacrylamide. **D**, **E** Treatment of linear and circular mRNA with endo- and exonucleases (**D** RNase H−RH and **E** RNase R−RR, respectively) to confirm the circular topology of the reaction products. **A–E** Data presented is representative of one independent experiment.

production. Depending on the circularization method used, the resulting mixture may contain remnants of unreacted linear precursor, polymerized linear and circular side products such as dimers and concatemers, excised intron fragments, nicked circRNA, or splint templates that can activate the innate immune response[6,35]. To establish optimal methods for identifying and purifying chem-circRNA, we first reviewed established methods from the literature. Then, we conducted a detailed examination and optimization of selected methods, leading to significant improvements and insightful findings.

The yields of RNA circularization and the homogeneity of circRNAs were determined based on electrophoretic analyses. Initially, we attempted to resolve linear and circRNAs on denaturing agarose gel. However, we typically observed poor resolution or overlap between linear and circular species of corresponding weight, which has also been reported previously[5,6,14,36]. Consequently, we turned our attention to denaturing polyacrylamide gel electrophoresis (PAGE). By varying both the degree of cross-linking of the polyacrylamide (PAA) and the final concentration of the AA/MBAA (acrylamide/*N, N'*-methylenebisacrylamide) blend, we determined the optimal density and cross-linking degree of polyacrylamide gels for the best migration and separation of linear and circRNA (Fig. 4, Supplementary Table 3). In all studied cases, the migration speed of the circular RNA macromolecules in polyacrylamide gel was significantly slower than that of linear precursors of corresponding weight (Fig. 4A) or high-molecular-weight (HMW, 3000–6000 nt) linear RNA molecules (Fig. 4B, C). A higher gel density (20% PAA) with a cross-linking degree of 5% (19:1 AA/MBAA) favored the separation of short linear mRNAs and their circularization products (RNA_{01}, 35 nt) (Fig. 4A). A lower gel percentage, corresponding to an increase in pore size, enhanced the migration rate of nucleic acids, as demonstrated for RNA_{03} (276 nt) and RNA_{04} (760 nt) on a 15% and 6% PAA gel, respectively. Conversely, a higher degree of cross-linking (19:1 AA/MBAA) significantly inhibited the migration of $circRNA_{03}$ (276 nt) and $circRNA_{04}$ (760 nt). Reducing the degree of cross-linking to 2.3% (38:1 AA/MBAA) increased the migration rate of circRNA while maintaining substantial separation between linear and circular RNA topologies. Such pronounced differences in nucleic acid migration are primarily attributed to variations in secondary structure rather than molecular weight. Through these experiments, we demonstrated that by manipulating gel density (from 20 to 4% PAA) and cross-linking degree (from 19:1 to 99:1 AA/MBAA ratio), one can achieve separation of linear and circular RNA species up to 4000 nt (Fig. 4; Supplementary Fig 7, Supplementary Table 3). High cross-linking degrees and high gel density enable the separation of short RNAs, whereas lower density and cross-linking degree gels are required for the efficient separation of long RNAs (for details, see Supplementary Table 3). Using these conditions, we could access the composition of the reaction mixtures in a simple, precise, and reproducible manner.

On the other hand, the topology of circRNAs can be readily verified by treating them with endonucleases and exonucleases, including RNase H and RNase R[3,37,38]. Digestion of intact chem-circRNA with oligonucleotide-guided RNase H predominantly produced a single band, in contrast to the nicking of its linear precursor, which yielded two split products of lower molecular weight (Fig. 4D). RNase R, with 3′ to 5′ exonuclease activity, eliminates linear contaminants from circRNA preparations[3,4]. Due to the unique closed-loop structure, circRNAs remain resistant to RNase R digestion, which has been used for circRNAs enrichment. We found that chem-circRNAs are essentially also resistant to RNase R, as the RNase-treated circularization reaction yielded solely the chem-circRNA band (Fig. 4E). However, when applying RNase R digestion for chem-circRNAs enrichment, we observed that both the quality of the circRNA sample and the presence of some sequence and structural elements may affect the selectivity of the reaction (Supplementary Fig. 8). Digestion of RP-HPLC-purified mixtures of circular and linear RNA significantly increased the selectivity of RNase R towards the linear RNA species (Supplementary Fig. 8A). To investigate the resistance of chemically circularized RNAs to RNase R, we conducted RNase R digestion on three chem-$circRNA_{11}$ variants with different linker lengths [$(EDA)RNA_{11}$, $(EP_5)RNA_{11}$ and $(EP_5Cap)RNA_{11}$], as well as an enz-$circRNA_{11}$ [$(p)RNA_{11}$] with a phosphodiester bond at the junction site. We established that introducing a chemical linker in chem-$circRNA_{11}$ does not preclude the use of RNase R for chem-circRNA enrichment (Supplementary Fig. 8B). However, we also observed undesired degradation of chem-$circRNAs_{11}$. This issue may be resolved by optimizing RNase R digestion conditions, such as enzyme concentration incubation times or buffer composition.

To obtain high-purity circRNA samples on a smaller scale (for in vitro studies), we employed PAGE separation of linear and circular RNA. The chem-circRNA molecules were resolved on PAA gel and extracted using either the crush-and-soak method or electroelution (Supplementary Fig. 9). We found that the UV spectra of the isolated material differed greatly, indicating that crush-and-soak isolation leads to contamination of RNA with PAA. In contrast, electroelution yielded chem-circRNA of high purity (>85% on PAGE) with an acceptable UV spectrum (Supplementary Fig. 9A–C). Given that RNAs separated on denaturing agarose gels are reportedly non-translatable due to interactions between denaturants (formaldehyde) and nucleotide monomers[39], we investigated the translational activity of circRNAs

https://doi.org/10.1038/s41467-025-61775-1

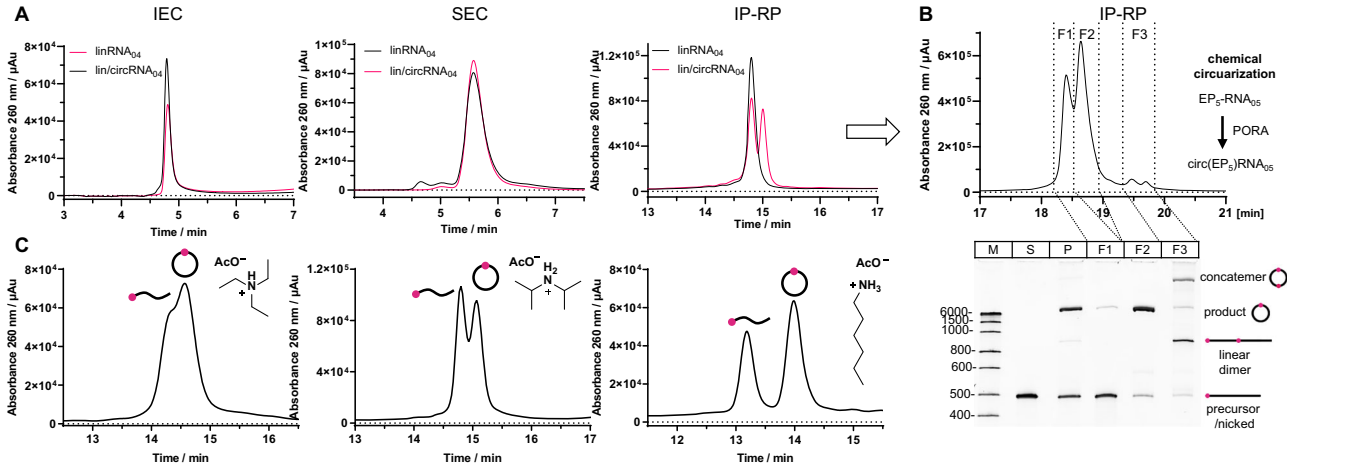

Fig. 5 | Analysis and purification of circRNA using high-performance liquid chromatography (HPLC). A Samples of linear (p)RNA_{04} and crude post-circularization mixture containing linear (p)RNA_{04} and circ(p)RNA_{04}, (RNA_{04} 760 nt) were analyzed using different HPLC methods: ion-exchange (IEC), size-exclusion (SEC), and reversed-phase (RP). **B** IP-RP-HPLC separation of linear and $circRNA_{05}$ (578 nt) followed by PAGE analysis of collected fractions. Column and buffers as in A—IP-RP (Supplementary Information). Fractions F1 contains mostly precursor RNA; F2 contains the circular product of high purity; F3 includes linear dimers and concatemers. **C** Resolution of linear (lower retention time) and circular (higher retention time) RNA_{06} (598 nt) using IP-RP-HPLC with different ion-pairing reagents: triethylammonium acetate (TEAA), diisopropylammonium acetate (DIPAA), or n-hexylammonium acetate (HAA). **A**–**C** For purification/separation conditions please see Supplementary Information.

isolated from polyacrylamide gels (Supplementary Fig 9D). The circ(EP_5Cap)RNA_{12} and reference circular RNA obtained by PIE splicing strategy ($circRNA_{16}$-PIE) were purified via PAGE/electroelution or RNase R treatment to compare their translational activity in cultured cells. The biological impact of circRNA isolation was assessed in three cell lines (A549, HEK293T, HepG2). Regardless of the circRNA sample, total protein levels were comparable between the isolation methods (Supplementary Fig 9D).

Another possible method for chem-circRNA purification is isolation from the reaction mixture by high-performance liquid chromatography (HPLC). We investigated this in three modes: ion-exchange chromatography (IEC), size-exclusion chromatography (SEC), and reversed-phase chromatography (RP) (Fig. 5). Previous studies utilized SEC for isolating circularization products from self-catalytic precursors using permuted intron-exon (PIE) methodology[5,6,14]. SEC can be effective in such a scenario because during the transesterification reaction, the linear precursor eliminates chain fragments corresponding to sequences of autocatalytic introns, contributing to a decrease in molecular mass. However, in our hands, SEC did not facilitate the separation of linear and circular RNA molecules of the same size and sequence (such as chem-circRNA and its precursor or the desired circRNA and nicked product). Successful separation of RNA molecules based on their topology was achieved only in RP mode in the presence of ion-pairing agents (IP-RP) (Fig. 5B). Optimal separations were achieved at 60 °C temperature on polystyrene divinylbenzene copolymer resin in the presence of n-hexylammonium acetate and acetonitrile (Fig. 5C). Notably, the IP-RP-HPLC method was effective only for RNAs shorter than 800 nt; for longer RNAs, the retention times for circular and linear forms were too similar (Supplementary Fig 10). The recovery rates ranged from 50% to 70%, with higher sample amounts leading to improved recovery. No correlation was observed between peak separation and the injected sample amount for the tested amounts ranging from 25 to 60 µg. The combination of IP-RP-HPLC and PAGE provided us with a set of tools to precisely analyze circularization reactions and isolate the desired circRNA products with high purity.

Translation of chemically modified circRNA

After establishing a robust methodology for preparing chem-circRNAs, we investigated the influence of chem-circRNA sequence and chemical modifications on its biological activity. Our study focused on two key aspects: (i) the biological stability and translational activity of chemically circularized mRNA and (ii) the incorporation of the N7-methylguanosine (m^7G) cap structure and poly(A) tract into chemically circularized mRNAs and their functional implications. To investigate the translational properties and structure-activity relationship of chem-circRNA, we designed and synthesized a series of precursor sequences (RNA_{09}, RNA_{11}–RNA_{15}), encoding a *Gaussia* luciferase, flanked by 5′ and 3′ untranslated regions (UTRs) and poly(A) sequences (Table 1).

Circularization was achieved using two strategies: chemical circularization employing the PORA method or enzymatic ligation via T4 RNA ligase II. The precursors for chemical circularization were obtained by IVT using EP_5AG and EP_5Cap (Fig. 1B) as initiators to yield (EP_5)RNA and (EP_5Cap)RNA, respectively, and were subsequently circularized via the PORA method to afford circ(EP_5)RNA and circ(EP_5Cap)RNA. For enzymatic circularization affording circ(p)RNA, the linear RNA precursors with a 5′ monophosphate [(p)RNA] were generated using guanosine monophosphate (GMP) as the transcription initiator (Fig. 1A). To assess the biological activity, circular RNAs and their linear RNA precursors—each bearing the corresponding 5′ end modification—were transfected into four distinct cell lines (A549, HEK 293 T, HepG2 and HeLa). Before the key experiments, we confirmed that PORA conditions do not impact the translational activity of mRNA using a mock mRNA (RNA_{09}) treated with PORA conditions but without the oxidation step (Supplementary Fig. 11).

Next, the translational activity of chemically circularized RNA constructs was evaluated to determine whether the introduction of the EP_5 chemical linker influences circRNA functionality (Fig. 6A, B). For this analysis, we employed a model mRNA (RNA_{12}) containing the encephalomyocarditis virus (EMCV) internal ribosome entry site (IRES) sequence, which facilitates cap-independent translation initiation, followed by coding sequence only. Given that the purity of circRNA preparations was between 85% to 95%, we aimed to exclude any significant contribution of residual linear precursors to the overall translational output. The applied mRNA design minimized potential biases arising from residual linear RNA species, as the lack of 3′ UTR and poly(A) leads to their rapid degradation and low translational activity. Thus, this model system ensured that any observed translational activity was primarily derived from circRNAs rather than residual

https://doi.org/10.1038/s41467-025-61775-1

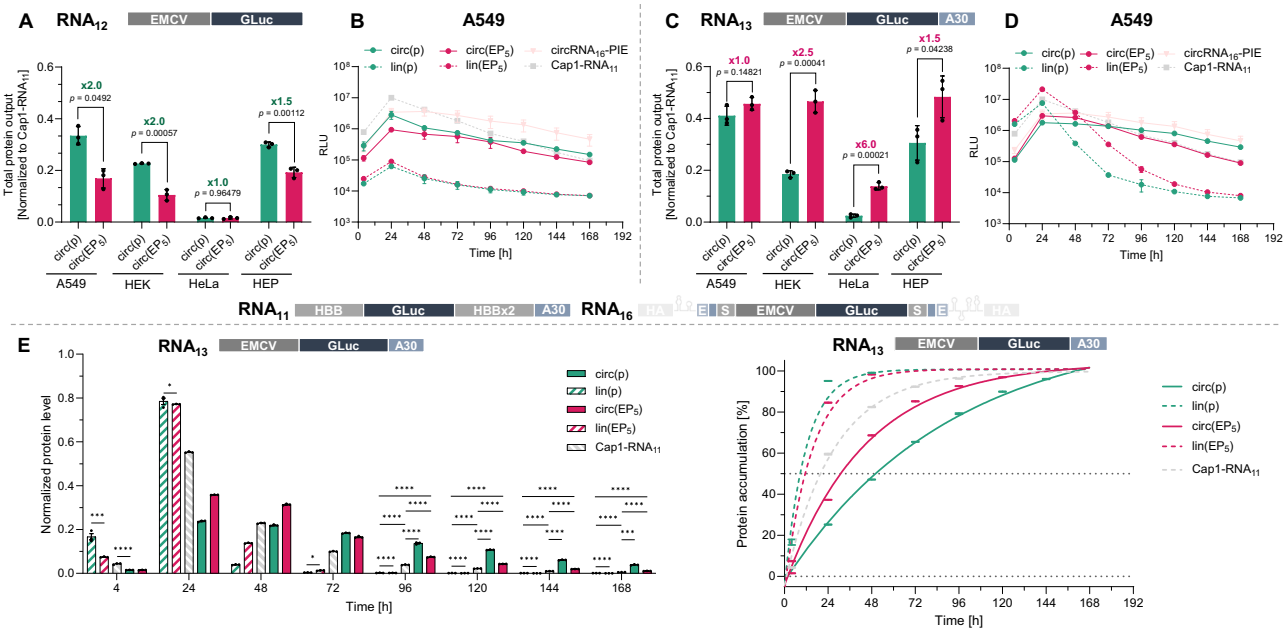

Fig. 6 | Chemically circularized RNAs (chem-circRNAs) are compatible with translation. A–E Translation activity and protein production profiles of linear and circular mRNAs based on two sequence designs: RNA_{12} (**A**, **B**) and RNA_{13} (**C**–**E**), both containing EMCV IRES elements upstream of the GLuc coding region. Circular RNAs were generated from linear precursors bearing either a 5′-monophosphate (p-) or ethylenediamine motif (EP_5). **A**, **C** Show total protein output measured in A549, HEK293T (HEK), HeLa, and HepG2 (HEP) cells over 168 h post-transfection, normalized to canonical Cap1-RNA_{11} (=1). **B**, **D** Show time-course of luciferase activity in A549 cells transfected with circ(p), circ(EP_5), lin(p), lin(EP_5), and control RNAs. **A**–**D** Data represent mean ± SD from three biological replicates ($n = 3$). **A**, **C** *P* values were calculated using unpaired Student's *t* test. **E** Shows normalized protein levels obtained from RNA_{13} calculated as a protein level at a specific timepoint divided by the total protein collected over 168 h. The bars (left graph) represent the relative levels of the reporter protein in the cell culture medium, determined at the indicated time points and normalized to the level obtained for the reference canonical mRNA (Cap1-RNA_{11}), means ± SEM, $n = 3$, * $P < 0.05$, *** $P < 0.001$, **** $P < 0.0001$, ordinary one-way ANOVA with Tukey's multiple comparisons test (4 h, 96 h, 120 h, 144 h, 168 h) or Kruskal–Wallis test with Dunn's multiple comparisons test (24 h, 48 h, 72 h). The right graph shows time-dependent protein accumulation (percentage of protein produced at all timepoints from 0 h up to the specific timepoint) calculated for each timepoint and fitted to a one-phase decay curve to determine the protein production half-life (the time after which half of the total protein level was reached). Source data are provided as a Source Data file.

linear RNA. To ensure a fair comparison of the translational activities of linear and circular RNAs of the same sequence (Fig. 6A), we confirmed in a separate qPCR experiment that the circular and linear RNA species of the same sequence are transfected with similar efficiencies (Supplementary Fig. 12). PIE-derived $circRNA_{16}$-PIE and a linear mRNA optimized for cap-dependent translation (Cap1-RNA_{11}) served as additional references (Fig. 6B). As anticipated, the translational activity of circ(EP_5)RNA_{12} was substantially higher than that of its linear precursor (Fig. 6B). Notably, chemically circularized circ(EP_5)RNA_{12} showed comparable translational activity and stability to its enzymatically circularized counterpart circ(p)RNA_{12} (Fig. 6A, B), underscoring the biocompatibility of the internucleotide linkage formed upon chemical circularization.

Next, we examined the influence of poly(A) tract, on the durability of protein expression and the translational activity of chem-circRNA analogs. The effect of a 30-nucleotide poly(A) sequence was assessed using $circRNA_{13}$ (Fig. 6C–E). As expected, the stability of linear precursors was enhanced by the poly(A) tract, leading to a transient surge in protein expression within the first 24 h post-transfection, followed by a rapid decline (Fig. 6D, E). The chemically and enzymatically circularized variants of the same sequence—circ(EP_5)RNA_{13} and circ(p)RNA_{13}—provided sustained protein production, showing similar durability to circRNAs lacking a poly(A) sequence [circ(p)RNA_{12} and circ(EP_5)RNA_{12}] (Fig. 6B, D). Notably, the $circRNA_{13}$ analogs exhibited prolonged expression profiles, with estimated protein production half-lives ranging from 29 to 50 h, significantly exceeding those of their linear counterparts (8–11 h) (Fig. 6E, Supplementary Fig 13A). Comparing the results obtained for RNA_{12} and RNA_{13} we concluded that, unlike what is observed for linear mRNAs, adding a poly(A) tract downstream of the coding sequence does not increase circRNA durability. Importantly, both chemically and enzymatically circularized RNAs displayed a protein production profile similar to that of $circRNA_{16}$-PIE, which incorporates a custom-designed spacer at the splicing site (Fig. 6B, D)[5,6].

We next examined how adding m^7G cap structure to circRNAs with IRES-EMCV will affect their translational activity. We hypothesized that enabling these two distinct translation initiation mechanisms in circRNAs could enhance protein production. To test this, we chemically circularized mRNAs containing a 5′EP_5Cap, followed by the EMCV IRES and GLuc reporter sequences alone (RNA_{12}) or in combination with additional downstream elements, including a poly(A) tract (RNA_{13}), the HBB 3′ UTR (RNA_{14}), or the HBB 3′ UTR followed by a poly(A) tract (RNA_{15}) (Fig. 7 and Supplementary Fig 14). A linear Cap1-RNA_{11} construct served as a reference.

Incorporating the cap structure into chemically circularized RNA [circ(EP_5Cap)RNA_{12} and circ(EP_5Cap)RNA_{13}] increased the protein output compared to the enzymatically circularized counterparts [circ(p)RNA_{12} and circ(p)RNA_{13}], with an average enhancement of 4-fold for RNA_{12} and 5-fold for RNA_{13}, irrespective of the presence of a downstream poly(A) tract (Fig. 7A, C). Adding a 3′ UTR alone or 3′ UTR followed by a poly(A) tract to the mRNA sequence, amplified the difference between capped circRNAs [circ(EP_5Cap)RNA_{14} and circ(EP_5Cap)RNA_{15}] and their enzymatically circularized counterparts [circ(p)RNA_{14} and circ(p)RNA_{15}], yielding 6.5–21-fold and 6.5–17-fold increases for RNA_{14} and RNA_{15}, respectively (Fig. 7E, G). However, when compared to circ(EP_5Cap)RNA_{12} and circ(EP_5Cap)RNA_{13}, RNA_{14} and RNA_{15} showed lower overall protein production (Fig. 7A, C, E, G). This suggested that the 3′ terminal elements essential for linear RNAs (3′

https://doi.org/10.1038/s41467-025-61775-1

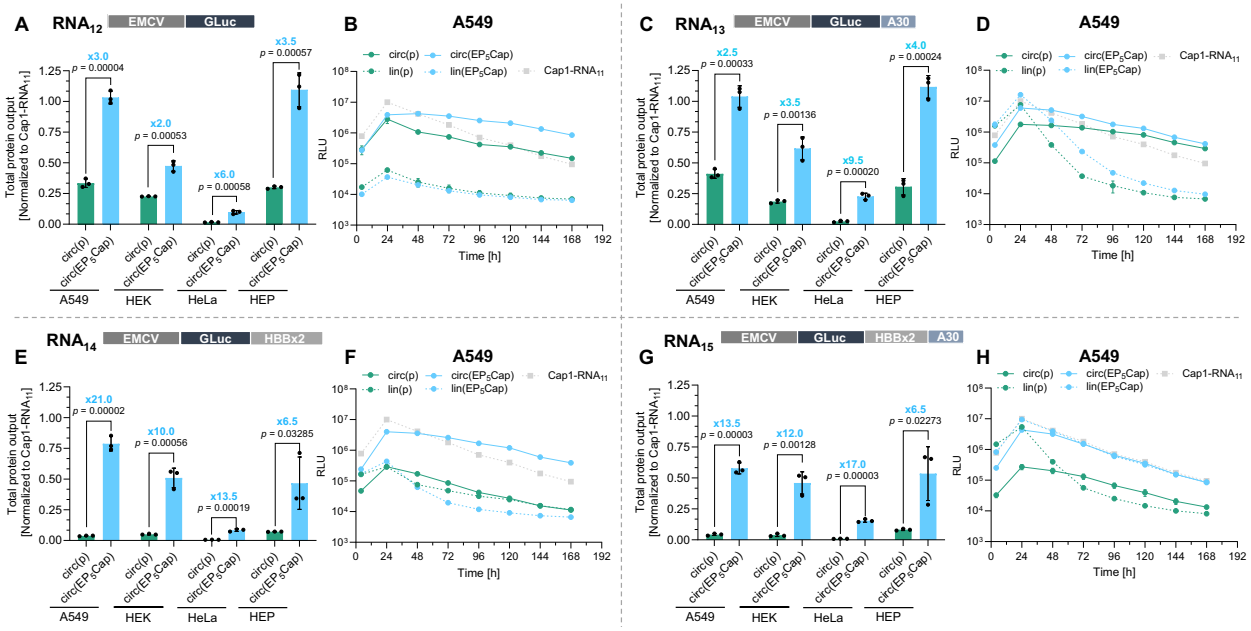

Fig. 7 | Chem-circRNAs with endocyclic cap structure have superior translational properties. A–H Translation activity and protein expression profiles of enzymatically circularized and chem-circRNAs derived from four RNA templates (RNA_{12}–RNA_{15}) in A549, HEK 293 T (HEK), HeLa, and HepG2 (HEP) cells. Circular RNAs were generated from linear precursors containing either a 5′ monophosphate (p-) or an EP_5Cap structure and encoded GLuc. **A**, **C**, **E**, **G** Show total protein output from transfected cells after 168 h, normalized to expression from the canonical linear Cap1-RNA_{11} (=1); **B**, **D**, **F**, **H** Show time-course of GLuc expression in A549 cells transfected with indicated constructs. **A**, **C**, **E**, **G** Data represent mean ± SD of three biological replicates ($n = 3$), *P* values were calculated using unpaired Student's *t* test. Source data are provided as a Source Data file.

UTR and poly(A)) are not beneficial for circRNA design, even if combined with the endocyclic cap. Importantly, most chem-circRNAs carrying an endocyclic cap [circ(EP_5Cap)RNA_{12}, circ(EP_5Cap)RNA_{13}, circ(EP_5Cap)RNA_{14}] showed increased durability and sustained protein production compared to their linear counterparts (Fig. 7B, D, F). However, in an RNA sequence optimized for the cap-dependent translation (i.e., containing both a 3′ UTR (HBB) and 30-nt poly(A) tract), the protein production profiles of circular RNA and linear RNAs were very similar (Fig. 7H).

We further investigated the effect of incorporating the m^7G cap on biological activity of circRNA using RNA sequences optimized for cap-dependent translation (i.e., without IRES; Fig. 8). To that end, we circularized capped mRNA (EP_5Cap) bearing a minimal 5′ UTR (Kozak), a 3′ UTR derived from the human β-globin (HBB) gene, and a 30-nt poly(A) tract (RNA_{09}) (Fig. 8). The translational activity of chemically circularized circ(EP_5Cap)RNA_{09} and enzymatically circularized circ(p)RNA_{09} constructs was assessed against linear Cap1-RNA_{11} serving as a reference (Fig. 8A, C). Introducing the cap structure into circRNA_{09} [circ(EP_5Cap)RNA_{09}] led to a striking 13–370-fold increase in protein levels compared to its enzymatically circularized counterpart circ(p)RNA_{09} (Fig. 8A). Notably, the overall protein output observed for circ(EP_5Cap)RNA_{09} was higher than observed for circRNAs containing the IRES-EMCV sequence ($RNA_{12\text{-}15}$) (Figs. 7A, C, E, G and 8A). However, the overall translational activity and durability of capped circRNA_{09} [circ(EP_5Cap)RNA_{09}] were similar to its linear precursor [lin(EP_5Cap)RNA_{09}] (Fig. 8B). Overall, these findings further support our observation regarding the influence of mRNA sequence architecture on protein output. Specifically, as an RNA sequence becomes increasingly optimized for cap-dependent translation, the translational profile of circRNA appears to converge with that of its linear counterpart, diminishing the advantages typically associated with circularization.

To verify if the endocyclic cap in circRNA can engage in the cap-dependent translation mechanism, we evaluated the expression of circ(EP_5Cap)RNA_{09}, circ(p)RNA_{09}, and circ(p)RNA_{15} in a cell-free system (rabbit reticulocyte lysate, RRL) in the presence of a cap-dependent translation inhibitor (m^7Gp_sppG dinucleotide, Fig. 8D)[40,41]. As expected, increasing concentration of the inhibitor led to a progressive reduction in reporter protein levels from circ(EP_5Cap)RNA_{09}, whereas circ(p)RNA_{15}, which contains an IRES sequence, remained unaffected. These findings strongly suggest that the endocyclic m^7G cap structure in chem-circRNA_{09} is functional and engages in the cap-dependent translation mechanism.

Next, we investigated whether our chemical circularization approach is compatible with mRNA body modifications commonly used to reduce undesired immunogenicity of in vitro transcribed mRNAs. To that end, N1-methylpseudouridine ($m^1\Psi$) is among the most critical modifications in therapeutic mRNA, as it has been shown to reduce activation of cytosolic and toll-like receptors (TLRs), thereby lowering cellular immune response and mRNA-associated toxicity[42]. However, the incorporation of $m^1\Psi$ and other noncanonical nucleobases can disrupt the function of RNA elements such as IRES sequences or autocatalytic introns by altering their secondary structure[6]. To determine whether an endocyclic cap structure could functionally substitute for the IRES element and support the translation of circRNA containing the $m^1\Psi$ modification, we generated $m^1\Psi$-modified circRNAs by either chemical or enzymatic circularization. The resulting circRNAs (variants of RNA_{15}) were transfected into four cell lines to assess their translational activity (Fig. 8E–H). As expected, IRES-dependent translation of enzymatically circularized RNA [circ(p)RNA_{15} (EMCV+$m^1\Psi$)] was abolished, likely due to $m^1\Psi$-induced disruption of the IRES secondary structure and consequent loss of function (Fig. 8E, G). In contrast, the chemically circularized capped RNA [circRNA_{09} (Cap+$m^1\Psi$)], which contained $m^1\Psi$ and the HBB UTR, remained translationally active, albeit at a reduced level compared to its unmodified counterpart (Fig. 8E, F). A similar reduction in translational activity was observed upon incorporating of $m^1\Psi$ into linear Cap1-RNA_{11} (Fig. 8E, H). In human monocyte-derived dendritic cells, all tested mRNAs but the ones containing virus-derived IRES sequences show negligible reactogenicity, as evidenced by the secretion of CXCL8 (Supplementary Fig. 15). Collectively, these results demonstrate that

https://doi.org/10.1038/s41467-025-61775-1

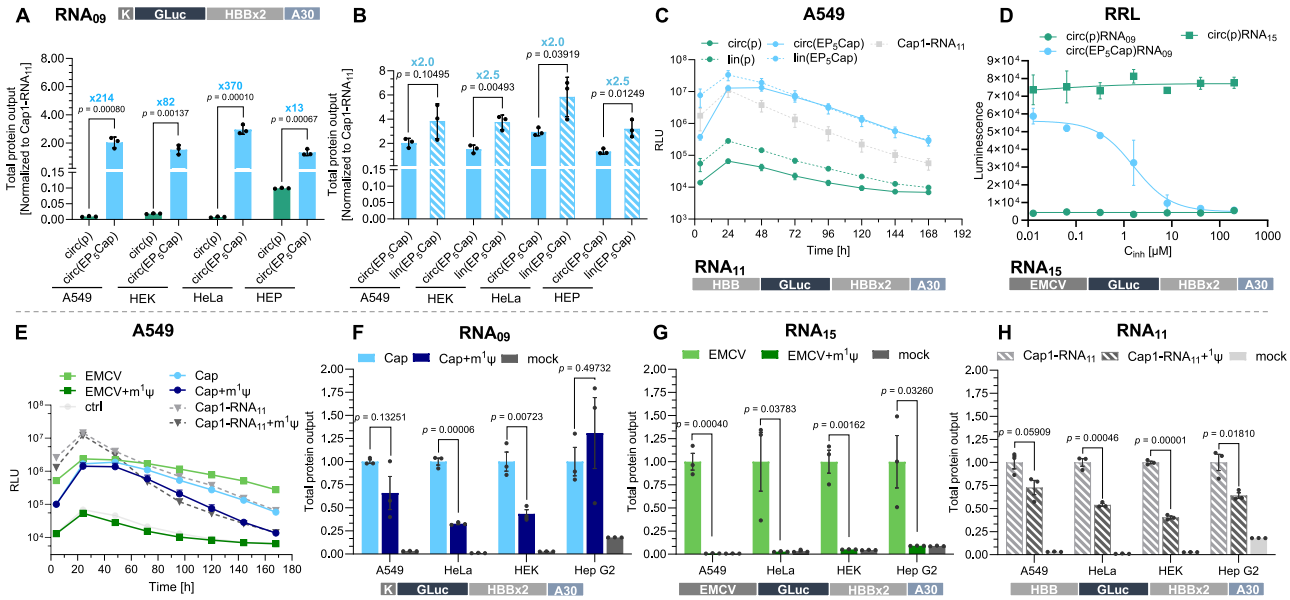

Fig. 8 | Chem-circRNAs containing endocyclic cap engage in the cap-dependent translation. A, **B** Show total protein output from circRNA$_{09}$ and linear (EP$_5$Cap)RNA$_{09}$ constructs in A549, HEK293T (HEK), HeLa, and HepG2 (HEP) cells transfected with circular RNAs derived from linear precursors bearing either a 5′ monophosphate (p-) [circ(p)RNA$_{09}$] or an EP$_5$Cap structure [circ(EP$_5$Cap)RNA$_{09}$]. Protein expression was measured as secreted GLuc activity accumulated over 168 h and normalized to the level obtained with canonical Cap1-RNA$_{11}$ (=1). **C** Shows the time-course of GLuc expression in A549 cells transfected with circ(p)RNA$_{09}$, circ(EP$_5$Cap)RNA$_{09}$, respective linear precursors, and linear Cap1-RNA$_{11}$. **D** Shows in vitro translation of circ(p)RNA$_{09}$, circ(EP$_5$Cap)RNA$_{09}$, and circ(p)RNA$_{15}$ in rabbit reticulocyte lysate (RRL) in the presence of the cap-dependent translation inhibitor (m^{7}Gp$_s$ppG), demonstrating inhibition of translation and supporting a cap-dependent translation mechanism[40,41]. Chem-circ RNAs containing N1-methylpseudouridine can be translationally active (**E**–**H**). Cells were transfected with circ(EP$_5$Cap)RNA$_{09}$ (Cap), circ(p)RNA$_{15}$ (EMCV), Cap1-RNA$_{11}$, and their respective counterparts containing N1-methylpeudouridine (+m^{1}Ψ). **E** Shows the time-course of GLuc expression from circRNAs (circ(EP$_5$Cap)RNA$_{09}$ and circ(p)RNA$_{15}$) and linear Cap1-RNA$_{11}$ over 168 h in A549 cells. **F**–**H** Show the total protein output from four cell lines (A549, HeLa, HEK, HepG2) transfected with circ(EP$_5$Cap)RNA$_{09}$/circ(EP$_5$Cap)RNA$_{09}$ + m^{1}Ψ (**F**), circ(p)RNA$_{15}$/circ(p)RNA$_{15}$ + m^{1}Ψ (**G**), linear Cap1-RNA$_{11}$/Cap1-RNA$_{11}$ + m^{1}Ψ (**H**), harvested at 168 h post-transfection. In each **F**–**H**, values are normalized to the signal from the corresponding uridine-containing mRNA. **A**, **B**, **F**, **G**, **H** Data represent mean ± SD of three biological replicates ($n = 3$), P values were calculated using unpaired Student's t test. Source data are provided as a Source Data file.

the chemical circularization method is compatible with RNA base modifications and highlight its potential for optimizing circRNAs' biological activity in therapeutic applications.

Finally, we have verified if chem-circRNAs obtained by the PORA method are compatible with translation in vivo. To that end, we prepared two chem-circRNAs, RNA$_{18}$ and RNA$_{19}$, encoding human erythropoietin. These RNAs were formulated into LNPs (Supplementary Fig. 16) and injected into C57BL/6 mice, followed by blood collection at 6, 24, and 48 h and determination of hEPO levels by ELISA (Fig. 9). We observed a significantly higher overall protein output for chem-circ RNAs, compared to their linear counterparts, confirming both the biocompatibility of the internucleotide linkage formed during circularization and the advantage of chem-circRNAs over their linear counterparts. However, the overall protein output and translation durability were relatively low, emphasizing the need for further optimization of the chem-circRNA sequence.

Discussion

In this work, we report the first method for the chemical circularization of in vitro transcribed (IVT) mRNA. Exogenously delivered circRNA represents a promising drug modality due to its extended lifespan in the cytosol. Since circRNAs lack free ends, they are not susceptible to exonuclease-mediated degradation, which is the main pathway for the bulk removal of cytoplasmic RNA[2,43]. To date, the most well-characterized methods for circularizing linear mRNA involve enzymatic ligation (RNA or DNA ligases) and ribozymatic methods based on self-splicing introns (Fig. 1)[5,8–15]. Chemical methods have been limited to short RNA sequences applicable to rolling circle amplification (RCA) of short peptides[44]. Our group has been involved for many years in developing chemical modifications of RNA ends. In this work, we leveraged this experience to develop a method of joining modified 5′ and 3′ ends of in vitro transcribed RNA, i.e. to chemically circularize full-length mRNAs. We were inspired by recent observations, made by us and others[26,34] that even in long RNA macromolecules, the 5′ and 3′-ends are usually sufficiently close to each other to enable fluorescence energy transfer (<10 nm), which should mean they are also close enough to efficiently undergo an intramolecular chemical reaction. As a result, our study describes a convenient method for obtaining chemically circularized RNAs (chem-circRNAs) based on a direct and selective chemical reaction called PORA (Periodate Oxidation and Reductive Amination). The starting material for this reaction is RNAs obtained by a standard in vitro transcription in the presence of transcription primers carrying an ethylenediamine motif. PORA is performed on the RNA product in a one-pot two-step reaction relying on simple reagents, taking less than 2 h and providing conversions in the range of 35–63%.

Notably, our methodology enables incorporating chemical modifications into circRNAs previously incompatible with this modality. For example, the translational activity of circRNAs reported in the literature depends on IRES sequences, highly structured regions within the 5′ UTR, that recruit ribosomes. Although m^{1}Ψ can be incorporated into these sequences, it disrupts their secondary structure, abolishing translational activity. In contrast, our circRNA design, which features an endocyclic cap structure, supports cap-dependent translation and, hence, can be modified with m^{1}Ψ without dramatically compromising the translational activity of the circRNA.

Chemical circularization represents an attractive alternative to existing methods for mRNA circularization, particularly for full-length coding mRNAs. In comparison to ribozyme-based approaches utilizing permuted group I catalytic introns, chemical circularization produces

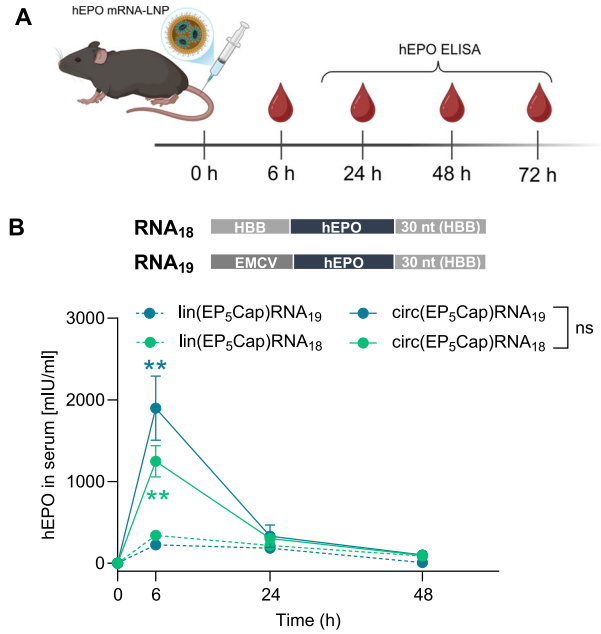

Fig. 9 | In vivo translatability of chemically circularized RNA for human erythropoietin (hEPO). A C57BL/6 female mice were intravenously inoculated with 1 μg of SM-102 -based LNP-formulated RNA. Blood was collected at the indicated time points to measure hEPO concentration with ELISA. Experimental setup. Created in BioRender. Chmieliński, S. (2025) https://BioRender.com/txhelkn. **B** hEPO concentration in serum over time, means ± SD, $n = 5$. Green stars: $P < 0.01$ for circ(EP_5Cap)RNA_{18} vs each of the linear RNA group; teal stars: $P < 0.01$ for circ(EP_5Cap)RNA_{19} vs each of the linear RNA group; ns—not significant (circ(EP_5Cap)RNA_{18} vs circ(EP_5Cap)RNA_{19}), 2 way ANOVA with Tukey's multiple comparisons test. Source data are provided as a Source Data file.

a simplified impurity profile (Fig. 5 vs. Supplementary Fig. 5) and does not require magnesium ions during the reaction, which may contribute to higher RNA homogeneity.

Using simple 35 nt RNA models (RNA_{01} and RNA_{02}), we demonstrated that circularization yields are predominantly dependent on the local secondary structure of RNA (end-to-end distance) rather than its length (Fig. 2). We further showed that circularization is equally efficient for RNA of various lengths and sequences, up to almost 4000 nt long. A reduction in circularization efficiency was observed for longer RNAs and those with unstructured 3′ ends (incorporating 3′ terminal polyA tracts), probably because of higher conformational flexibility. This issue was addressed by secondary structure control with oligonucleotide DNA splints, achieving circularization efficiencies ranging from 35% to 60%, even for complex macromolecular RNA constructs (Table 1). We also developed methods that enable efficient separation of chem-circRNAs from their unreacted linear precursors and provided molecular tools to verify the structure and homogeneity of chem-circRNAs. Our results demonstrate that chem-circRNAs undergo translation in living cells, similarly, to enzymatically obtained circRNAs, and remain translationally active in a mouse model. Moreover, the duration of expression in cells for most chem-circRNA analogs was extended compared to their linear precursors (Fig. 6E). We also investigated the impact of elements required for cap-dependent translation, such as the m^7G cap and the poly(A) tract, on the durability of protein production and the translational activity of our chem-circRNA analogs. Adding m^7G cap increased the translational activity of chem-circRNAs, although the effect was sequence dependent. We demonstrated that the endocyclic cap in chem-circRNA maintains its functionality, as evidenced by enhanced protein production compared to unmodified circRNAs (Fig. 7) and susceptibility to inhibition by compounds targeting the cap-binding translation factor, eIF4E (Fig. 8D).

We investigated the effect of introducing an EP_5Cap structure to RNAs containing an internal ribosome entry site (IRES) in the 5′ untranslated region (UTR). In our experiments, we employed the well-characterized EMCV IRES, which has been widely used in both linear and circular RNAs. However, the design of our circular RNAs could potentially be improved by exploring other IRES sequences with higher activity, such as those derived from HCV or HRV-B3 [45,46].

Overall, our data reveal that chemical circularization is compatible with RNA base-modifications and that the endocyclic cap moiety could serve as an alternative to IRES for promoting circRNA translation (Fig. 8E–H). However, further extensive optimization of chem-circRNA sequences and chemical structures is crucial to fully realize the potential of this methodology. Nonetheless, to our best knowledge, this work describes several unprecedented achievements in RNA circularization: (i) the chemical circularization of mRNA encoding full-length protein, (ii) the chemical circularization of IVT RNA, (iii) the development of circular RNAs that undergo cap-dependent translation, and (iv) the circularization of $m^1\Psi$-modified RNA. While this work was under review, two other manuscripts independently showing the creation of circular RNAs equipped with m^7G and their superior translational activity were published, highlighting that chemical modifications and topology alterations are the future directions for the development of circRNA field[47,48]. Unlike our work, these methods were based on the enzymatic ligation approach. Compared to enzymatic ligation and autocatalytic circularization, our approach allows for site-selective introduction of RNA chain modifications simply by adding an analog of a substrate for RNA polymerase during the IVT reaction. This gives users the freedom of choice of chemical modifications that could help expand the repertoire of known and tested circRNA modifications. In light of that, we believe this work opens an unexplored avenue for capped circular RNA and potentially a new generation of RNA therapeutics. Still, more research on sequence optimization and other aspects of chem-circRNA design is needed to fully embrace the potential of this technology.

Methods

Software and tools used

The MFE secondary structure model of the mRNA sequences was predicted with RNAfold web server, with energy parameters: RNA parameters (Turner model, 2004). The three-dimensional RNA models were created with the RNA Composer web server tool. The circular mRNA content was determined by densitometric analysis of the raw PAGE images using ImageJ or CLIQS (Core Laboratory Image Quantification Software).

Preparation of linear 5′ end modified and unmodified mRNA as circularization precursors

The synthesis of the respective IVT initiators and intermediates is detailed in the Supplementary Information.

Unmodified and modified linear mRNA precursors were synthesized by in vitro transcription from a linearized plasmid DNA template using T7 RNA Polymerase, HC (Thermo) followed by treatment with DNase I (Thermo). mRNA was purified using a silica-based column followed by RP-HPLC. After HPLC purification, the recovered RNA represents 75–90% of the initial crude mRNA.

Chemical circularization

An aqueous solution of the precursor RNA (25–50 μg in 490 μl, ~140 μM) was diluted with buffer (70 μl, 800 mM KH_2PO_4, 200 mM NaCl, pH 7.0) and incubated at 65 °C for 5 min, followed by cooling to r.t. After 10-15 min at r.t., a fresh solution of sodium periodate (70 μl, 10 mM) was added, and the reaction mixture was immediately placed in the dark and incubated at 25 °C for 30 min. A fresh solution of

sodium cyanoborohydride (70 μl, 200 mM) was added to the final volume of 700 μL, and the incubation was continued for 90 min. The crude circRNA product was purified using a silica-based column (Monarch RNA cleanup kit, 50 μg, NEB) followed by RP-HPLC. After HPLC purification, the recovered RNA represented 50–70% of the initial crude mRNA. For additional purification and removal of linear RNA, the product was either treated with RNase R as described below (see Section RNase R digestion) or isolated via electroelution (for details see Supplementary Information).

Chemical circularization with complementary splint

The reaction was carried out following the procedure outlined above, with the modification that a complementary oligonucleotide (~11 μl, 10 μM, 1.5 eq, see Supplementary Table 2 for sequence) was employed.

RNase R digestion

A solution of RNA (43 μl, 10 μg) was incubated at 65 °C for 5 min and rapidly cooled in the ice bath. After 5 min at 0-4 °C, RNase R buffer ×10 (5 μl, 200 mM Tris-HCl, 1 M KCl, 1 mM $MgCl_2$, pH 7.5, ABM), RiboLock RNase inhibitor (1.25 μl, 40 U/μl, Thermo), and RNase R (1 μl, 10 U/μl, ABM) were added. After 30 min of incubation at 37 °C the products of digestion were analyzed with PAGE directly or isolated from the reaction mixture using Monarch RNA cleanup kit (10 μg, NEB).

RNase H nicking analysis

A solution of circular RNA (2.60 μl, 500 ng) in water (17.8 μl) was heated at 70 °C for 5 min in the presence of a DNA probe (0.85 μl, 6 eq., 10 μM, 5′CCTTCAGCTCGATGCGGTTCA 3′) and gradually cooled to 37 °C for 20 min. Next, RNase H buffer ×10 (2.5 μl, 50 mM Tris-HCl, 75 mM KCl, 3 mM $MgCl_2$, 10 mM DTT, pH 8.3), and RNase H (1.25 μl, 1 U/μl, Thermo) were added to final volume of 25 μl. After 15 min of incubation at 37 °C the products of digestion were directly analyzed with PAGE.

Translation inhibition in RRL system

Flexi Rabbit Reticulocyte Lysate (4 μL, Promega) was diluted with 4 μL solution containing amino acid mixture (100 μM), KOAc (500 mM), and $MgCl_2$ (2.5 mM), and incubated for 1 h at 30 °C. Next, 1 μL of RNA (100 ng/μl) mixed with 1 μL of m^7GpsppG (0.32–200 μM) was added to 8 μL of the lysate mixture and incubated for 1 h at 30 °C. Next, the reaction was immediately placed into a microplate reader (Synergy H1, BioTek), 50 μL of h-coelenterazine in 1× PBS was added and the luminescence was measured at 25 °C. The assay was performed in duplicate to calculate the mean and standard error (SEM).

Cell culture and transfection (A549, HEK 293 T, HeLa, Hep G2)

One day before transfection, 8×10^3 cells were seeded per well of a 96-well plate and incubated under standard conditions (37 °C, 5% CO_2, saturating humidity). Transfection was performed with Lipofectamine Messenger MAX (Invitrogen, Waltham, MA, USA), according to the manufacturer's instructions. Each RNA variant (65 ng) was transfected in triplicate. At appropriate time points, 20 μL of medium from each well was withdrawn to test the amount of produced protein, and the remaining medium was completely replaced with a fresh one. The amount of luciferase released into the medium was analyzed using the GLuc GLOW Assay (NanoLight Technologies, Norman, OK, USA) reagents, according to the manufacturer's instructions using an EnVision plate reader (Perkin Elmer, Waltham, MA, USA)

In vivo experiment

Mice. The experiments were carried out in 10–12-week-old (~25 g) female C57BL6/cmdb under the protocols approved by the II Local Ethical Committee for Experiments on Animals in Warsaw, Poland (WAW2/111/2024). All experiments were conducted in accordance with the Directive of the European Parliament and Council No. 2010/63/EU on the protection of animals used for scientific purposes. Mice were obtained from the Breeding Facility of the Medical University of Bialystok, Bialystok, Poland. All animals were maintained in a specific pathogen-free (SPF) environment in the individually ventilated cages (IVC) under the conditions of a 12-h day/night cycle, 55% humidity and +22 °C air temperature with unrestricted access to food and drinking water.

Formulation

The respective linear mRNAs and their circular counterparts were generated according to the general procedure described in the Supplementary Information, with the exception that circRNAs were enriched using RNase R digestion.

The mRNA in 100 mM citrate buffer (pH 4) and lipid mixture (25 mM in ethanol) containing 50 mol% SM-102, 10 mol% DSPC, 38.5 mol% cholesterol, and 1.5 mol% DMG-PEG 2000 were combined to form lipid nanoparticles using the NanoAssemblr Spark (Precision Nano-systems). The obtained mRNA-LNPs were diluted in dPBS, and the buffer was exchanged by concentrating the solution through 50 kDa spin filters (MilliporeSigma, UFC505024) to remove ethanol. Concentrations and encapsulation efficiency of mRNA were determined using the Quant-it Ribo-Green RNA Assay Kit (ThermoFisher, R11490). The mean particle size and particle size distribution of the LNPs were analyzed by DLS using a Zetasizer Ultra (Malvern Instruments Ltd., Worcestershire, UK).

In vivo human erythropoietin mRNA expression studies

All mice were randomly assigned to experimental groups ($n = 5$ C57BL/6 mice per group). Each mouse received intravenously 100 μL of LNP-encapsulated human erythropoietin (hEPO) mRNA (1 μg per mouse). Blood samples were collected via cheek pouch from submandibular veins at 6, 24, 48, and 72 h after mRNA-LNPs injection. The blood was allowed to clot at room temperature for 30 min, and the serum was separated by centrifugation at 10,000×*g* for 10 min. Human EPO levels in serum were quantified using an ELISA kit (Invitrogen, Human EPO ELISA Kit, # BMS2035-2) according to the manufacturer's instructions.

Statistical analysis

Statistical analysis was performed using GraphPad Prism version 9. Figures were generated using the same software and statistical significance was determined using appropriate tests. For normal data distribution evaluation the Shapiro-Wilk test was used. Details of all remaining statistical tests used are provided in the figures' captions.

Reporting summary

Further information on research design is available in the Nature Portfolio Reporting Summary linked to this article.

Data availability

All data supporting the findings of this study are available within the paper and its Supplementary Information. Complete DNA sequences, detailed descriptions of chemical syntheses, characterization of chemical compounds, experimental procedures involving in vitro transcription, RNA circularization and preparation, nucleolytic assays, FRET probes, cell culture, and cell-free experiments are provided in the Supplementary Information. Source data are provided with this paper.

References

1. Rohner, E., Yang, R., Foo, K. S., Goedel, A. & Chien, K. R. Unlocking the promise of mRNA therapeutics. *Nat. Biotechnol.* **40**, 1586–1600 (2022).
2. Garneau, N. L., Wilusz, J. & Wilusz, C. J. The highways and byways of mRNA decay. *Nat. Rev. Mol. Cell Biol.* **8**, 113–126 (2007).
3. Suzuki, H. et al. Characterization of RNase R-digested cellular RNA source that consists of lariat and circular RNAs from pre-mRNA splicing. *Nucleic Acids Res.* **34**, e63 (2006).

4. Suzuki, H. & Tsukahara, T. A View of Pre-mRNA Splicing from RNase R Resistant RNAs. *Int. J. Mol. Sci.* **15**, 9331–9342 (2014).
5. Wesselhoeft, R. A., Kowalski, P. S. & Anderson, D. G. Engineering circular RNA for potent and stable translation in eukaryotic cells. *Nat. Commun.* https://doi.org/10.1038/s41467-018-05096-6 (2018).
6. Wesselhoeft, R. A. et al. RNA circularization diminishes immunogenicity and can extend translation duration in vivo. *Mol. Cell* **74**, 508–520.e504 (2019).
7. Enuka, Y. et al. Circular RNAs are long-lived and display only minimal early alterations in response to a growth factor. *Nucleic Acids Res.* **44**, 1370–1383 (2016).
8. Chen, X. & Lu, Y. Circular RNA: biosynthesis in vitro. *Front. Bioeng. Biotechnol.* **9**, 787881 (2021).
9. Dolinnaya, N. G. et al. Oligonucleotide circularization by template-directed chemical ligation. *Nucleic Acids Res.* **21**, 5403–5407 (1993).
10. Fedorova, O. A., Gottikh, M. B., Oretskaya, T. S. & Shabarova, Z. A. Cyanogen bromide-induced chemical ligation: mechanism and optimization of the reaction conditions. *Nucleosides Nucleotides* **15**, 1137–1147 (1996).
11. Nakamoto, K. et al. Chemically synthesized circular RNAs with phosphoramidate linkages enable rolling circle translation. *Chem. Commun.* **56**, 6217–6220 (2020).
12. Rigden, J. E. & Rezaian, M. A. In vitro synthesis of an infectious viroid: analysis of the infectivity of monomeric linear CEV. *Virology* **186**, 201–206 (1992).
13. Chen, C.-Y. & Sarnow, P. Initiation of protein synthesis by the eukaryotic translational apparatus on circular RNAs. *Science* **268**, 415–417 (1995).
14. Qu, L. et al. Circular RNA vaccines against SARS-CoV-2 and emerging variants. *Cell* **185**, 1728–1744.e1716 (2022).
15. Kaufmann, G., Klein, T. & Littauer, U. Z. T4 RNA ligase: substrate chain length requirements. *FEBS Lett.* **46**, 271–275 (1974).
16. Litke, J. L. & Jaffrey, S. R. Highly efficient expression of circular RNA aptamers in cells using autocatalytic transcripts. *Nat. Biotechnol.* **37**, 667–675 (2019).
17. Kumar, A. et al. *Extensive in Vitro and in Vivo Protein Translation Via in Situ Circularized RNAs* (Cold Spring Harbor Laboratory, 2022).
18. Ford, E. & Ares, M. Synthesis of circular RNA in bacteria and yeast using RNA cyclase ribozymes derived from a group I intron of phage T4. *Proc. Natl Acad. Sci. USA* **91**, 3117–3121 (1994).
19. Puttaraju, M. & Been, M. Group I permuted intron-exon (PIE) sequences self-splice to produce circular exons. *Nucleic Acids Res.* **20**, 5357–5364 (1992).
20. Sinha, T., Panigrahi, C., Das, D. & Chandra Panda, A. Circular RNA translation, a path to hidden proteome. *WIREs RNA* https://doi.org/10.1002/wrna.1685 (2022).
21. Lei, M., Zheng, G., Ning, Q., Zheng, J. & Dong, D. Translation and functional roles of circular RNAs in human cancer. *Mol. Cancer* https://doi.org/10.1186/s12943-020-1135-7 (2020).
22. Ramanathan, A., Robb, G. B. & Chan, S.-H. mRNA capping: biological functions and applications. *Nucleic Acids Res.* **44**, 7511–7526 (2016).
23. Yang, Y. & Wang, Z. IRES-mediated cap-independent translation, a path leading to hidden proteome. *J. Mol. Cell Biol.* **11**, 911–919 (2019).
24. Koch, A., Aguilera, L., Morisaki, T., Munsky, B. & Stasevich, T. J. Quantifying the dynamics of IRES and cap translation with single-molecule resolution in live cells. *Nat. Struct. Mol. Biol.* **27**, 1095–1104 (2020).
25. Kim, B., Seol, J., Kim, Y. K. & Lee, J.-B. Single-molecule visualization of mRNA circularization during translation. *Exp. Mol. Med.* https://doi.org/10.1038/s12276-023-00933-1 (2023).
26. Mamot, A. et al. Ethylenediamine derivatives efficiently react with oxidized RNA 3′ ends providing access to mono and dually labelled RNA probes for enzymatic assays and in vivo translation. *Nucleic Acids Res.* **50**, e3 (2022).
27. Fan, X., Yang, Y., Chen, C. & Wang, Z. Pervasive translation of circular RNAs driven by short IRES-like elements. *Nat. Commun.* https://doi.org/10.1038/s41467-022-31327-y (2022).
28. Chen, C.-K. et al. Structured elements drive extensive circular RNA translation. *Mol. Cell* **81**, 4300–4318.e4313 (2021).
29. Mullgan, M. J. et al. Phase I/II study of COVID-19 RNA vaccine BNT162b1 in adults. *Nature* **586**, 589–593 (2020).
30. Coleman, T. M., Wang, G. & Huang, F. Superior 5′ homogeneity of RNA from ATP-initiated transcription under the T7 ϕ2.5 promoter. *Nucleic Acids Res.* **32**, e14 (2004).
31. Lorenz, R. et al. ViennaRNA Package 2.0. *Algorithms Mol. Biol.* https://doi.org/10.1186/1748-7188-6-26 (2011).
32. Sarzynska, J., Popenda, M., Antczak, M. & Szachniuk, M. RNA tertiary structure prediction using RNAComposer in CASP15. *Proteins* **91**, 1790–1799 (2023).
33. Popenda, M. et al. Automated 3D structure composition for large RNAs. *Nucleic Acids Res.* https://doi.org/10.1093/nar/gks339 (2012).
34. Lai, W. et al. mRNAs and lncRNAs intrinsically form secondary structures with short end-to-end distances. *Nat. Commun.* https://doi.org/10.1038/s41467-018-06792-z (2018).
35. Karikó, K., Muramatsu, H., Ludwig, J. & Weissman, D. Generating the optimal mRNA for therapy: HPLC purification eliminates immune activation and improves translation of nucleoside-modified, protein-encoding mRNA. *Nucleic Acids Res.* https://doi.org/10.1093/nar/gkr695 (2011).
36. Abe, B., Wesselhoeft, R., Chen, R., Anderson, D. & Chang, H. Circular RNA migration in agarose gel electrophoresis. *Mol. Cell* **82**, 1768–1777 (2022).
37. Starke, S. et al. Exon circularization requires canonical splice signals. *Cell Rep.* **10**, 103–111 (2015).
38. Dodbele, S., Mutlu, N. & Wilusz, J. Best practices to ensure robust investigation of circular RNAs: pitfalls and tips. *EMBO Rep.* https://doi.org/10.15252/embr.202052072 (2021).
39. Masuda, N., Ohnishi, T., Kawamoto, S., Monden, M. & Okubo, K. Analysis of chemical modification of RNA from formalin-fixed samples and optimization of molecular biology applications for such samples. *Nucleic Acids Res.* **27**, 4436–4443 (1999).
40. Perzanowska, O., Smietanski, M., Jemielity, J. & Kowalska, J. Chemically modified poly(A) analogs targeting PABP: structure activity relationship and translation inhibitory properties. *Chemistry* https://doi.org/10.1002/chem.202201115 (2022).
41. Kowalska, J. et al. Synthesis and characterization of mRNA cap analogs containing phosphorothioate substitutions that bind tightly to eIF4E and are resistant to the decapping pyrophosphatase DcpS. *RNA* **14**, 1119–1131 (2008).
42. Nance, K. D. & Meier, J. L. Modifications in an emergency: the role of N1-methylpseudouridine in COVID-19 vaccines. *ACS Cent. Sci.* **7**, 748–756 (2021).
43. Chen, L. & Yang, L. Regulation of circRNA biogenesis. *RNA Biol.* **12**, 381–388 (2015).
44. Abe, N. et al. Rolling circle translation of circular RNA in living human cells. *Sci. Rep.* https://doi.org/10.1038/srep16435 (2015).
45. Chen, R. et al. Engineering circular RNA for enhanced protein production. *Nat. Biotechnol.* **41**, 262–272 (2023).
46. Unti, M. J. & Jaffrey, S. R. Highly efficient cellular expression of circular mRNA enables prolonged protein expression. *Cell Chem. Biol.* **31**, 163–176 (2024).
47. Fukuchi, K. et al. Internal cap-initiated translation for efficient protein production from circular mRNA. *Nat. Biotechnol.* https://doi.org/10.1038/s41587-025-02561-8 (2025).
48. Chen, H. et al. Chemical and topological design of multicapped mRNA and capped circular RNA to augment translation. *Nat. Biotechnol.* https://doi.org/10.1038/s41587-024-02393-y (2024).

Acknowledgements
This project was supported by Virtual Research Institute Łukasiewicz Research Network—PORT Polish Center for Technology Development project "Horizon for Excellence in messenger RNA applications in immunOncology"[HERO] financed by the Polish Science Fund.

Author contributions
J-.J. and J.K. conceived the research and acquired funding for this project, supervision, Writing—Review & Editing. A.M. and M.W.K. contributed equally. J.J., J.K., A.M., and M.W.K.: Conceptualization. A.M. and M.W.K.: Methodology, Validation, Investigation, Visualization, Resources. A.M., M.W.K., and J.K.: Writing—Original Draft. K.C. and Z.P.: Investigation, Validation. D.N.: In vivo data analysis. K.F.: Investigation, Visualization, Resources. T.S., A.A.R., and M.S.G.: Investigation, Resources. M.W., A.D., and K.S.: Resources. D.N. and J.G.: Writing—Review & Editing, Supervision. All authors have approved the final version of the paper.

Competing interests
J.K., J.J., A.M., M.W.K., M.W., A.A.R., K.F., K.C., D.N., and J.G. are co-inventors of patent application related to chemical circularization of RNA (EP23461592.0A). The remaining authors declare no competing interests.

Additional information
Supplementary information The online version contains supplementary material available at https://doi.org/10.1038/s41467-025-61775-1.

Correspondence and requests for materials should be addressed to Joanna Kowalska or Jacek Jemielity.

Peer review information *Nature Communications* thanks the anonymous reviewer(s) for their contribution to the peer review of this work. A peer review file is available.

Reprints and permissions information is available at http://www.nature.com/reprints

Publisher's note Springer Nature remains neutral with regard to jurisdictional claims in published maps and institutional affiliations.

Open Access This article is licensed under a Creative Commons Attribution-NonCommercial-NoDerivatives 4.0 International License, which permits any non-commercial use, sharing, distribution and reproduction in any medium or format, as long as you give appropriate credit to the original author(s) and the source, provide a link to the Creative Commons licence, and indicate if you modified the licensed material. You do not have permission under this licence to share adapted material derived from this article or parts of it. The images or other third party material in this article are included in the article's Creative Commons licence, unless indicated otherwise in a credit line to the material. If material is not included in the article's Creative Commons licence and your intended use is not permitted by statutory regulation or exceeds the permitted use, you will need to obtain permission directly from the copyright holder. To view a copy of this licence, visit http://creativecommons.org/licenses/by-nc-nd/4.0/.

© The Author(s) 2025